# Simulating $C_3$-to-CAM transition under ancient atmospheric conditions

Devlina Sarkar and Sudip Kundu*

Department of Biophysics, Molecular Biology and Bioinformatics, University of Calcutta

92, APC Road, Kolkata 700009, India

*Corresponding author email: skbmbg@caluniv.ac.in

ORCID IDs- Devlina Sarkar: https://orcid.org/0009-0006-3979-4380

Sudip Kundu: https://orcid.org/0000-0003-1235-2540

Word count of the main section- 1934

No of figures in the main text- 2 (All the figures should be published in colour)

11 separate supporting information files (9 excel files, 1 sbml file and 1 text file) with the main SI word file

**Abstract**

Crassulacean Acid Metabolism (CAM) plants can survive in arid environment. CAM is hypothesized to evolve from $C_3$ metabolism about 20 to 30 million years ago (MYA) when the Earth faced declining atmospheric $CO_2$ concentration ($[CO_2]_a$), increasing aridity and decreasing temperature. Understanding whether and how these atmospheric changes favour $C_3$-to-CAM transition will help in engineering CAM into crop plants to tackle the threat of global climate change. Our simulations of plant cellular metabolism under the changing atmospheric conditions of ancient time observe $C_3$-to-CAM transition, capture possible temporal alterations of active metabolic pathways and further confirm that both the reduced $[CO_2]_a$ and increased water scarcity associated with higher aridity, can act as evolutionary agents, driving the $C_3$-to-CAM transition. Although the predicted elevated $[CO_2]_a$ of future reveals a reversion towards $C_3$-like behaviour, drought always favours CAM regardless of $[CO_2]_a$ and temperature levels. Moreover, a minimum oxygen concentration is needed to support higher nocturnal respiration, necessary for CAM.

**Main text**

Crassulacean Acid Metabolism (CAM) plants can survive in arid environment. Time-calibrated phylogenies and large-scale carbon isotope ($\delta^{13}C$) studies suggest that CAM is evolved from $C_3$ about 20-30 million years ago (MYA) (Heyduk, 2022; Sage *et al.*, 2023). Evidences also suggest that during early-Eocene (56 MYA) to early-Miocene (20 MYA), atmospheric $CO_2$ concentration ($[CO_2]_a$) declined from 700-1000 ppm to about 200 ppm (Bellasio *et al.*, 2021; Sage *et al.*, 2023), Earth's surface temperature (T) decreased from ~35ºC to ~22ºC (Passchier *et al.*, 2013; Judd *et al.*, 2024); and aridification increased (Passchier *et al.*, 2013; Wang *et al.*, 2016) (i.e. relative humidity (RH) decreased from an initial value of ~67% in middle-Miocene (Jahren *et al.*, 2003)). Researchers hypothesized that the above-mentioned atmospheric changes during ancient times favour the evolution of CAM (Sage *et al.*, 2023). Previous experimental efforts explored the physiological (Guan *et al.*, 2020) and molecular

changes (Kong *et al.*, 2020), altered gene expressions (Heyduk *et al.*, 2019; Shen *et al.*, 2022), transcriptomic (Cushman *et al.*, 2008; Brilhaus *et al.*, 2016) and proteomic (Guan *et al.*, 2021) changes, the roles of different phytohormones in controlling stomatal behaviour (Wakamatsu *et al.*, 2021) etc., during $C_3$-to-CAM transition in different facultative CAM species (Winter & Holtum, 2024) under different stress conditions (Tan & Chen, 2023). The different expression levels of carbonic anhydrase genes in *Arabidopsis thaliana* leaves were also reported under different atmospheric $CO_2$ concentrations (Rudenko *et al.*, 2022). On the other hand, several computational efforts simulated the $C_3$-to-CAM transition only in MC either by forcefully restricting the daytime $CO_2$ uptake (Tay *et al.*, 2021) or gradually reducing transpirational water loss accompanied by a trade-off in phloem sap production (Töpfer *et al.*, 2020). Recently, we developed a dual-cell (GC and MC) diel metabolic model, coupled with a gas diffusion model which links the $CO_2$ uptake to transpirational water loss, depending on the temporal fluctuations of T and RH (Sarkar & Kundu, 2025). Simulation showed gradual reduction of the transpirational water loss shifts the metabolism from $C_3$ to CAM and at the same time, captured the temporally differential activities of several enzymes involved in different pathways of central carbon metabolism, during this transition. However, none of these studies addressed whether and how atmospheric changes during early-Eocene to early-Miocene might have driven the shift from $C_3$ metabolism to CAM. Such insights will help in engineering CAM into crop plants to tackle the threat of global climate change (Lim *et al.*, 2025)**.** To investigate this, we simulate our previously published six-phase GC-MC diel metabolic model (Sarkar & Kundu, 2025) of a plant leaf (**Supporting Information Fig. S1a**) using a constraint-based modelling approach (Flux Balance Analysis or FBA) (Orth *et al.*, 2010), under varying atmospheric conditions of that geological time period (**Supporting Information Fig. S1b-d**, for details, see Methods). Simulations observe $C_3$-to-CAM transition, capture possible temporal alterations of active metabolic pathways and further confirm that both the reduced $[CO_2]_a$ and increased water scarcity associated with higher aridity, can act as evolutionary agents, driving the $C_3$-to-CAM transition. While future's elevated $[CO_2]_a$ reveals a reversion towards $C_3$-like behaviour, drought always favours CAM regardless of $[CO_2]_a$ and temperature levels. Moreover, a minimum oxygen concentration is needed to support higher nocturnal respiration, necessary for CAM. Model files are provided in **Supporting Information Datasets S1** and **S2**.

At first, we simulate the model under the atmospheric condition of early-Eocene period with the average T of 35°C, RH of 70% and $[CO_2]_a$ of 800 ppm (**Supporting Information Fig. S1b-d**). Results confirm the important characteristics of a $C_3$ metabolism- such as $CO_2$ uptake only at daytime (Winter & Smith, 2022), malate storage at daytime in MC (Winter & Smith, 2022), early morning $K^+$ storage in GC (Daloso *et al.*, 2017) and sucrose storage in the later phases of the day in GC (Daloso *et al.*, 2017) etc.

Next, we gradually decrease the $[CO_2]_a$, T and RH until the values reach to 250 ppm, 22°C and 30% respectively, representing the atmospheric condition of the early-Miocene period and simulate the

model at each step (**Supporting Information Fig. S1b-d**). With this gradual reduction, the metabolism begins to exhibit key features of CAM (Winter & Smith, 2022) (**Supporting Information Dataset S3**)- i) $CO_2$ uptake at night (**Fig. 1a**) through nighttime GC-mediated stomatal opening (**Fig. 2e, Supporting Information Fig. S2**), ii) the increased activities of some $C_4$-like enzymes such as PEPC (phosphoenolpyruvate carboxylase) and MDH (malate dehydrogenase) at nighttime, whereas PEPCK (phosphoenolpyruvate carboxykinase) and NADP-ME (NADP-dependent malic enzyme) at daytime in MC (**Fig. 1b**); and iii) the increased daytime starch and nighttime malate storages in MC (**Fig. 1c**). Although nocturnal $CO_2$ uptake begins around 419 ppm (**Fig. 1a**), nighttime malate accumulation starts earlier (**Fig. 1c**). In response to decline in $[CO_2]_a$, plant initially adjusts its metabolism by limiting daytime $CO_2$ uptake and refixing respiratory $CO_2$ into malate at night. As $[CO_2]_a$ drops further, it starts taking atmospheric $CO_2$ at night to meet the total carbon requirement, in addition to respiratory $CO_2$ fixation (Griffiths *et al.*, 1989). CAM-like features gradually emerge as we move towards the Miocene, but the typical stomatal pattern with complete midday closure (Heyduk, 2022; Sarkar & Kundu, 2025) is not observed here. With CAM emergence, nocturnal respiration increases through elevated $O_2$ uptake, enhanced TCA fluxes (**Fig. 1d**, **Supporting Information Dataset S3, Supporting Information Note S1**), and increased mitochondrial ATP production, supplying essential energy for CAM. Additionally, simulation with restricted nighttime $O_2$ uptake reveals that increased nocturnal $O_2$ uptake is mandatory for CAM functioning, supporting the experimental observation that CAM requires elevated nocturnal respiratory rate and nocturnal $O_2$ consumption (Leverett & Borland, 2023). Interestingly, atmospheric $O_2$ concentration increased during that geological time period (Berner *et al.*, 2007), which probably supports the higher $O_2$ consumption and facilitated the emergence of CAM. Furthermore, as we move towards Miocene, there is an overall decrease in water-use efficiency (WUE) (**Fig. 1d**) due to increase in transpirational water loss. This result is consistent with earlier experimental reports suggesting that plants cope with the lower $[CO_2]_a$ by opening stomata and therefore stomatal conductance increases (Sage *et al.*, 2023). This consequently increases the transpiration rate and hence WUE decreases (Sage *et al.*, 2023).

Now, to identify the major atmospheric changes that favour $C_3$-to-CAM transition, we study the response of plant $C_3$ metabolism at higher $[CO_2]_a$ (800 ppm), but at different T (35ºC to 22 ºC) and RH (70% to 30%) (**Supporting Information Dataset S4**). Interestingly, we observe variations of T and RH, alone or in combination, are not sufficient to drive the $C_3$-to-CAM transition. We already show that the transition is favoured when changes in T and RH are coupled with lower $[CO_2]_a$ (**Fig. 1a**). Moreover, when we simulate the $C_3$ metabolism at reducing $[CO_2]_a$ only, keeping the T and RH fixed at 35ºC and 70% respectively, we observe the $C_3$-to-CAM transition (**Supporting Information Dataset S5**). These support the hypothesis that lower $[CO_2]_a$ during ancient times drives the $C_3$-to-CAM transition (Sage *et al.*, 2023).

We should note that we have not restricted the transpirational water loss in our earlier simulations to nullify the effect of reduced water loss during $C_3$-to-CAM transition established by previous studies (Töpfer *et al.*, 2020; Sarkar & Kundu, 2025). However, the increased aridity of early-Miocene is expected to be associated with reduced water availability and this water scarcity is also supported by the disappearance of lakes caused by aridity (Wang *et al.*, 2023) during various geological periods. As reduction in transpirational water loss is one of the ways to adapt and survive at water-stressed conditions, we gradually reduce the transpirational water loss at different points between early-Eocene to early-Miocene (**Supporting Information Fig. S1e**) and observe a metabolic shift to CAM regardless of whether $[CO_2]_a$ is high or low (**Supporting Information Dataset S3**). We also observe the shift in stomatal opening from day to night (**Fig. 2e, Supporting Information Fig. S2**), maximum $CO_2$ uptake at night (**Fig. 2a,b, Supporting Information Fig. S3**), higher activities of PEPC, PEPCK, MDH and NADP-ME (**Fig. 2c,d, Supporting Information Fig. S4**), and increased storages of starch and malate at day and night respectively (**Supporting Information Fig. S5**). These findings support the fact that water stress causes $C_3$-to-CAM transition even at higher $CO_2$ (Sage *et al.*, 2023). Various studies have suggested that both factors could drive the $C_3$-to-CAM transition (Silvera *et al.*, 2010; Sage *et al.*, 2023) and metabolic modelling also support the fact. However, the transition also demands substantial cellular and genetic modifications, which would further influence its evolutionary pathway. Interestingly, WUE increases when associated with the limitation in transpirational water loss at any point between early-Eocene and early-Miocene (**Supporting Information Fig. S6**). Moreover, as reduction in transpirational water loss (or water saving) diminishes with decline in $[CO_2]_a$, the extent of WUE improvement due to reduced water loss, is also reduced. It is also important to note that at higher $[CO_2]_a$, where higher water saving is possible, midday stomatal closure is observed (**Fig. 2e, Supporting Information Fig. S2**). The rank correlation values between reaction's flux and atmospheric changes from the early-Eocene to early-Miocene, or with reduced transpiration water loss at each point within this interval, indicate that MC metabolism shifts similarly during the $C_3$-to-CAM transition in both cases, whereas GC displays different patterns (**Supporting Information Dataset S6, Supporting Information Note S2**).

One of the major reasons of CAM emergence is reduced $[CO_2]_a$. However, after the industrial revolution, $[CO_2]_a$ increased roughly by 40%, from a value of 278 ppm (Asadi Zarch *et al.*, 2017). It continues to increase day by day and is predicted to increase further in near future (Asadi Zarch *et al.*, 2017). Model simulations under elevated $[CO_2]_a$ show enhanced daytime $CO_2$ uptake and reduced nocturnal fixation (**Supporting Information Table S1**), aligning with experimental findings (Sage *et al.*, 2023). Simulations under varying $[CO_2]_a$, T, and RH reveal that water loss rises with higher T, lower $[CO_2]_a$, and reduced RH (**Fig. 2f**). Moreover, for a fixed T and $[CO_2]_a$, imposing water-saving constraints along with reduced RH induces CAM, with greater nocturnal $CO_2$ uptake (**Fig. 2g, Supporting Information Dataset S7**). At high $[CO_2]_a$, plants shift $CO_2$ uptake to cooler nights due to

reduced transpirational water loss without reducing phloem sap. Whereas at low $[CO_2]_a$, limited $CO_2$ forces nocturnal uptake and further reduction in transpirational water loss compromises phloem sap production, reflecting a trade-off between water saving and phloem sap production (**Fig. 2g, Supporting Information Dataset S8**). For details, see **Supporting Information Note S3**.

In our model, $K_2$malate, KCl and sucrose are initially considered as osmolytes, with only sucrose permitted to transfer from MC to GC. We now extend the model to include additional osmolytes (nitrate, glucose, fructose and maltose) and transfer metabolites (glucose and malate) (**Supporting Information Dataset S9**). Simulations of this extended model indicate that, even with these inclusions, declining $[CO_2]_a$ and rising aridity consistently drive a metabolic shift toward CAM. While, MC shows similar metabolic patterns, GC shows variation in the storage patterns of these osmolytes for generating turgor pressure (**Supporting Information Note S4, Supporting Information Dataset S10**).

To summarize, although anatomical and physiological traits such as increased succulence in CAM plants (Lüttge, 2004), stomatal regulation by differential activities of signalling pathways (Blatt, 2000), mechanistic regulation of stomata (Blatt *et al.,* 2022), change in assimilation rate with atmospheric conditions (Rudenko *et al.,* 2022) etc., are not included in our model; this environment-coupled simple cellular metabolic model successfully reconstructs ancient conditions, captures the $C_3$-to-CAM transition driven by environmental changes during that geological time period and provide an initial useful framework to predict the possible differentially active metabolic pathways and quantitative estimations of relative flux values through those in the changing environment, a requisite for proper designing of abiotic stress tolerant cultivar.

## Materials and Methods

### Model Description

Our previously constructed time-resolved atmospheric factors coupled metabolic model of a plant leaf is used here (Sarkar & Kundu, 2025). Briefly, this is a six-phase dual-cell (GC-MC) metabolic model coupled with transpirational water loss and $CO_2$ uptake [see **Supporting Information Fig. S1a**, equation (1) and equation (2)]. The transpirational water loss from the system in each phase depends on different environmental parameters such as temperature (T) and relative humidity (RH) of that particular phase. The six phases, denoted as p1 to p6, represent different time intervals of a diel cycle: dawn (0-1 h), mid-day (1-11 h), afternoon (11-12 h), evening (12-13 h), night (13-23 h) and pre-dawn (23-24 h) respectively. Thus, the 24-hour time span of a complete diel cycle is divided into these six phases in a ratio of 1:10:1:1:10:1. The equations of a gas diffusion model are given below.

$$J_{CO_2,available} = D_{CO_2} \frac{n\pi R^2}{l+R_{mean}} ([\mathrm{CO_2}]_i - [\mathrm{CO_2}]_a) \quad (1)$$

Equation 1 represents the flux of $CO_2$ ($J_{CO_2,available}$) that can enter the leaf's internal airspace through a stomatal pore of radius R at a specific concentration of atmospheric $CO_2$ ($[CO_2]_a$) and temperature (T). Moreover, $[CO_2]_i$ represents the concentration of $CO_2$ inside the leaf, $D_{CO_2}$ is the diffusion coefficient of $CO_2$, n is the number of stomata per unit area of the leaf, $\pi R^2$ is the average area per stomatal pore, $l$ is the depth of stomatal pore and $R_{mean}$ is the mean radius which is added to the depth of the stomatal pore as a correction factor (Nobel, 2009). A plot of $D_{CO_2}$ values at some particular temperatures, listed in Appendix I (Nobel, 2009), gives us a straight-line graph, showed in **Supporting Information Fig. S7**. We use linear regression method to get the c (intercept) and m (slope) of that straight line. Now, we can calculate $D_{CO_2}$ values at specific temperatures of different phases of the diel cycle in different geological time periods. In a similar manner, we plot the internal $CO_2$ concentration of the leaf ($[CO_2]_i$) at different atmospheric $CO_2$ concentrations ($[CO_2]_a$) (>100 ppm) (Moss & Rawlins, 1963) and get the c (intercept) and m (slope) values using linear regression method. Using these values, we can calculate the $[CO_2]_i$ for any specific $[CO_2]_a$ value during early-Eocene to early-Miocene time period. The radius of the stomatal pore (R) at daytime is considered to be 7 µm with a basal value of 0.6 µm in the $C_3$ plant and the depth of the stomatal pore is considered to be twice the radius of the pore, assuming the pore to be circular, as used in our previously published work (Sarkar & Kundu, 2025). The number of stomata per $mm^2$ is considered to be 250, which is within the reported values, ranging from 45 to 720 (Hetherington & Woodward, 2003).

$$J_{H_2O} = k\left(c(T)^*_{i,H_2O} - c(T)^*_{a,H_2O}.RH\right).J_{CO_2,demand} \quad (2)$$

$$\text{where, } k = \frac{D^0_{H_2O}}{D^0_{CO_2}} . \frac{1}{[\mathrm{CO_2}]_i - [\mathrm{CO_2}]_a}$$

Equation 2 gives us the relationship between the water loss through transpiration and the $CO_2$ demand of the system depending on the T and RH in each phase throughout the diel cycle. The values of T and

RH for different phases of a diel cycle are estimated using a skewed sinus generator[7]. $c(T)^*_{H_2o}$ is the saturation concentration of water vapour, $D^0_{H_2o}$ and $D^0_{CO_2}$ are the standard diffusion coefficients of $H_2O$ and $CO_2$, and ($[CO_2]_i$ - $[CO_2]_a$) is the concentration difference of $CO_2$ inside and outside the leaf. We convert the values of concentration of $CO_2$ ($[CO_2]$) from ppm to μmol.m$^{-3}$ to use in our simulation.

The metabolisms of GC and MC are interlinked in this model in a very simple way. The accumulation of osmolytes in GC opens stomata. Equation 1 gives us the maximum flux of $CO_2$ that can enter the system depending on the size of stomatal pore, diffusion coefficients at different temperatures in different phases of the diel cycle and the concentration difference of $CO_2$ inside and outside the leaf. The amount of $CO_2$ entering each phase is further scaled by multiplying it with the duration of that phase. The entered $CO_2$ is available to 300 MCs and 1 GC in the internal space of the leaf as the ratio of MC to GC is considered to be 300, as used in our previous study (Sarkar & Kundu, 2025). On the other hand, MC supplies sucrose to GC, which ultimately helps in stomatal opening. Sucrose is allowed to transfer from MC to GC in phase 2 at daytime and in phase 5 at nighttime. The rate of solute accumulation (i.e, osmotic pressure or OP) is 1.928 μosmol.m$^{-2}$.s$^{-1}$ for 7 μm aperture size (Sarkar & Kundu, 2025). Assuming the photosynthetic capacity of GC to be 20%, the amount of sucrose transferred to GC is 80% of the OP, as previously used (Sarkar & Kundu, 2025). In the model, ions ($K^+$, $Cl^-$, $H^+$) can move in and out of GC during any phase of the day or night. However, experimental studies have shown that $K^+$ accumulates in GC primarily during early morning, while sucrose accumulation takes place later during the day (Lawson, 2009). Based on this, the transfer of $K^+$ from phase 2 to phase 3 is blocked in the model. The schematic representation of the model is shown in **Supporting Information Fig. S1a,** the model files are provided in the **Supporting Information Dataset S1** and **S2**; and all the other constraints are listed in the **Supporting Information Table S2.** The constraints, which we have taken from our previously published paper (Sarkar & Kundu, 2025), are based on various experimental observations (see references therein).

**Simulating the model with the changing atmospheric conditions during early-Eocene to early-Miocene period**

It is reported that $[CO_2]_a$ declined from 700-1000 to 200 ppm (Bellasio *et al.*, 2021; Sage *et al.*, 2023), T decreased from 35-22ºC (Passchier *et al.*, 2013; Judd *et al.*, 2024) and RH decreased (Passchier *et al.*, 2013; Wang *et al.*, 2016) during the early-Eocene to early-Miocene time period. There is no report about the values of RH in early-Eocene, whereas it is reported to be 67% in the middle Eocene (Jahren *et al.*, 2003). Several studies report the reduction of RH during this time interval (Passchier *et al.*, 2013; Wang *et al.*, 2016),but no specific value of RH for early-Miocene is available. Therefore, we consider the value of RH in early-Eocene to be 70%, slightly higher than that in middle-Eocene, and reduce it up-to 30%. We use some known physiological parameters for $C_3$ and CAM, already used in our previous work

(Sarkar & Kundu, 2025) and here, those are listed in **Supporting Information Table S2**. Some constraints like ratio of photon values in different phases of day, percentage of sucrose transferred from MC to GC in phase 2 and phase 5 etc., remain unchanged throughout the simulation from early-Eocene to early-Miocene time period. However, to implement the higher $CO_2$ concentration around RuBisCO in CAM, the ratio of carboxylase and oxygenase activities of RuBisCO is assumed to gradually increase from 3 to 5.15 (Tay *et al.*, 2021; Sarkar & Kundu, 2025) during this geological time period. As there was a majority of $C_3$ plants on the Earth before Oligocene or Miocene period (Sage *et al.*, 2023), we start the simulation using the constraints of $C_3$ in early-Eocene. There is no data available about the temporal variation of T and RH in ancient times and therefore, we assume the difference of max and min T and RH to be 10ºC and 10% respectively. Experimental evidences showed that the maximum stomatal apertures for basil and broad bean are 7 µm and 7.4 ± 2.3 µm respectively (Outlaw & De Vlieghere-He, 1992; Kang *et al.*, 2007). In our previously published model (Sarkar & Kundu, 2025), the starting aperture size of the simulation during all three daytime phases was set to 7 µm. A basal value of 0.6 µm during all the six phases was considered. But we did not impose any upper limit on stomatal opening. In the present study, however, we allow the aperture size to increase up-to 7µm, above the basal stomatal opening of 0.6 µm, resulting in a maximum aperture size of 7.6 µm at any phase, which lies within the reported experimental range. Here, a 2-step iteration method is used for simulating the model at a single geological time point. Steps for simulating the model under the changing atmospheric conditions between early-Eocene to early-Miocene time period are shown in **Supporting Information Fig. S1d**.

**Simulating the model with gradual reduction in transpirational water loss at each step of atmospheric changes between early-Eocene to early-Miocene period**

To check the effect of water scarcity at different geological time points, we simulate the model by gradually reducing transpirational water loss at every point of the atmospheric changes between early-Eocene to early-Miocene time period. Steps of this simulation are given in **Supporting Information Fig. S1e.**

**Calculating the correlation of the flux values through the metabolic reactions with changing atmospheric conditions and reduced transpirational water loss**

The rank correlation between the flux values of each reaction of the model- i) with the change in atmospheric conditions during early-Eocene to early-Miocene time period (gradual reduction in $[CO_2]_a$, T and RH) and ii) with the reduction in transpirational water loss at each point between that geological time period are calculated and the correlation values are provided in **Supporting Information Dataset S6.**

**Simulating the model at different $[CO_2]_a$, T and RH**

To check the response of plant metabolism in changing atmospheric conditions of future, we simulate the model by reducing the RH from 80% to 40% (with a decrement of 10%) at different combinations of $[CO_2]_a$ (800, 419 and 250 ppm) and T (26-35ºC with an increment of 1ºC). These simulations are performed- i) with unconstrained transpirational water loss and ii) with the transpirational water loss fixed at a value obtained by simulating the model with 80% RH for specific T and $[CO_2]_a$ combination. For example, at a given $[CO_2]_a$ of x ppm and T of y ºC, the first simulation involves reducing RH from 80% to 40% with unconstrained transpirational water loss. Whereas, in the second simulation, RH is similarly reduced from 80% to 40% at the same $[CO_2]_a$ and T; but in each step, transpirational water loss is fixed at the value obtained from simulating the model under $[CO_2]_a$ = x ppm, T = y ºC and RH = 80%. Here, we have started the simulation with full opening of stomata in all the six phases of diel cycle. Depending on the specific atmospheric condition, i.e., specific combination of $[CO_2]_a$, T and RH values, the phase-specific $CO_2$ import is predicted and the aperture size and OP are readjusted. Results are given in **Supporting Information Dataset S7** and shown in **Fig. 2f,g.**

**Simulating the model at $[CO_2]_a$ of 250 ppm with reduced phloem sap production**

At $[CO_2]_a$ of 250 ppm, we start with the rate of phloem sap production to be 0.259 $\mu mol.m^{-2}.^{-1}$. Then for each T and RH combination, we gradually decrease the production rate by 20%, keeping all the other constraints unchanged and simulate the model at each step using the 2-step iteration method (described earlier). Results are given in **Supporting Information Dataset S8** and shown in **Fig. 2g.**

**Flux Balance Analysis (FBA)**

We have used Flux Balance Analysis (FBA) (Orth *et al.,* 2010), a constraint-based modelling approach for simulating our model. In this approach, the reactions of the metabolic model are represented in the form of a stoichiometry matrix, **S** of size m x n, where m represents the number of metabolites and n represents the number of reactions present in the model. At steady state, the rate of production and the rate of consumption are equal for each internal metabolite in the model. This can be mathematically represented as,

$$\mathbf{Sv} = 0.$$

where, the vector **v** represents the flux through all the n number of reactions and **S** is the stoichiometry matrix.

The optimization problem can be defined as,

$$\text{maximize or minimize } \mathbf{z} = \mathbf{c}^T\mathbf{v}$$

where, **z** is the objective function, $\mathbf{c}^T$ is the transpose of a vector (**c**) of weights that indicate how much a reaction contributes to the objective, **v** is the vector of all fluxes.

The constraints on the flux values are given as,

$$\mathbf{c}_l \leq \mathbf{v} \leq \mathbf{c}_u$$

where, $\mathbf{v}$ is the vector of all fluxes, and $\mathbf{c}_u$ and $\mathbf{c}_l$ are the upper and lower bounds of fluxes, respectively.

The objective used in this study is parsimonious flux balance analysis (pFBA) to minimize the total absolute sum of fluxes (proxy of minimization of cellular economy). The scobra package (Shaw & Cheung, 2018) is used for simulations of FBA. The codes for all the simulations are given in **Supporting Information Dataset S11.**

**References**

**Asadi Zarch MA, Sivakumar B, Malekinezhad H, Sharma A**. **2017**. Future aridity under conditions of global climate change. *Journal of Hydrology* **554**: 451–469.

**Bellasio C, Quirk J, Ubierna N, Beerling DJ**. **2021**. Physiological responses to low CO2 over prolonged drought as primers for forest–grassland transitions. *Nature Plants* **8**: 1014–1023.

**Berner RA, VandenBrooks JM, Ward PD**. **2007**. Oxygen and evolution. *Science* **316**: 557–558.

**Blatt MR**. **2000**. Cellular signaling and volume control in stomatal movements in plants. *Annual review of cell and developmental biology* **16**: 221-241.

**Blatt MR, Jezek M, Lew VL, Hills A**. **2022**. What can mechanistic models tell us about guard cells, photosynthesis, and water use efficiency? *Trends in Plant Science* **27**: 166–179.

**Brilhaus D, Bräutigam A, Mettler-Altmann T, Winter K, Weber APM**. **2016**. Reversible burst of transcriptional changes during induction of crassulacean acid metabolism in Talinum triangulare. *Plant Physiology* **170**: 102–122.

**Cushman JC, Tillett RL, Wood JA, Branco JM, Schlauch KA**. **2008**. Large-scale mRNA expression profiling in the common ice plant, Mesembryanthemum crystallinum, performing C3 photosynthesis and Crassulacean acid metabolism (CAM). *Journal of Experimental Botany* **59**: 1875–1894.

**Daloso DM, Medeiros DB, dos Anjos L, Yoshida T, Araújo WL, Fernie AR**. **2017**. Metabolism within the specialized guard cells of plants. *New Phytologist* **216**: 1018–1033.

**Griffiths H, Ong BL, Avadhani PN, Goh CJ**. **1989**. Recycling of respiratory C02 during Crassulacean acid metabolism: alleviation of photoinhibition in *Pyrrosia piloselloides*. *Planta* **179**: 115-122.

**Guan Q, Kong W, Zhu D, Zhu W, Dufresne C, Tian J, Chen S**. **2021**. Comparative proteomics of Mesembryanthemum crystallinum guard cells and mesophyll cells in transition from C3 to CAM. *Journal of Proteomics* **231**: 104019.

**Guan Q, Tan B, Kelley TM, Tian J, Chen S**. **2020**. Physiological Changes in Mesembryanthemum crystallinum During the C3 to CAM Transition Induced by Salt Stress. *Frontiers in Plant Science* **11**: 283.

**Hetherington AM, Woodward & FI**. **2003**. The role of stomata in sensing and driving environmental change. *Nature* **424**: 901-908.

**Heyduk K**. **2022**. Evolution of Crassulacean acid metabolism in response to the environment: past, present, and future. *Plant Physiology* **190**: 19–30.

**Heyduk K, Hwang M, Albert V, Silvera K, Lan T, Farr K, Chang TH, Chan MT, Winter K, Leebens-Mack J**. **2019**. Altered gene regulatory networks are associated with the transition from C 3 to crassulacean acid metabolism in erycina (Oncidiinae: Orchidaceae). *Frontiers in Plant Science* **9**: 2000.

**Jahren AH, Silveira L, Sternberg L**. **2003**. Humidity estimate for the middle Eocene Arctic rain forest. *Geology*, **31**: 463-466.

**Judd EJ, Tierney JE, Lunt DJ, Montañez IP, Huber BT, Wing SL, Valdes PJ**. **2024**. A 485-million-year history of Earth's surface temperature. *Science (New York, N.Y.)* **385**: eadk3705.

**Kang Y, Outlaw WH, Fiore GB, Riddle KA**. **2007**. Guard cell apoplastic photosynthate accumulation corresponds to a phloem-loading mechanism. *Journal of Experimental Botany* **58**: 4061–4070.

**Kong W, Yoo MJ, Zhu D, Noble JD, Kelley TM, Li J, Kirst M, Assmann SM, Chen S**. **2020**. Molecular changes in Mesembryanthemum crystallinum guard cells underlying the C3 to CAM transition. *Plant Molecular Biology* **103**: 653–667.

**Lawson T**. **2009**. Guard cell photosynthesis and stomatal function. *New Phytologist* **181**: 13–34.

**Leverett A, Borland AM**. **2023**. Elevated nocturnal respiratory rates in the mitochondria of CAM plants: current knowledge and unanswered questions. *Annals of Botany* **132**: 855–867.

**Lim SD, Lomas JS, Islam M, Pérez-López A V., Kim SH, Petrusa LM, Yim WC, Cushman JC**. **2025**. Synthetic crassulacean acid metabolism (SynCAM) for improving water-use efficiency in plants. *Philosophical Transactions of the Royal Society B: Biological Sciences* **380**: 20240249.

**Lüttge U**. **2004**. Ecophysiology of Crassulacean Acid Metabolism (CAM). *Annals of Botany* **93**: 629–652.

**Moss DN, Rawlins SL**. **1963**. Concentration of Carbon Dioxide inside Leaves. *Nature*. **197**: 1320-1321.

**Nobel PS**. **2009**. Physicochemical and Environmental Plant Physiology. In: Physicochemical and Environmental Plant Physiology. Elsevier, 364–437.

**Orth JD, Thiele I, Palsson BO**. **2010**. What is flux balance analysis? *Nature Biotechnology* **28**: 245–248.

**Outlaw WH, De Vlieghere-He X**. **1992**. Transpiration Rate. An Important Factor Controlling the Sucrose Content of the Guard Cell Apoplast of Broad Bean. *Plant Physiology* **126**: 1716-1724

**Passchier S, Bohaty SM, Jiménez-Espejo F, Pross J, Röhl U, Van De Flierdt T, Escutia C, Brinkhuis H**. **2013**. Early eocene to middle miocene cooling and aridification of east antarctica. *Geochemistry, Geophysics, Geosystems* **14**: 1399–1410.

**Rudenko NN, Ignatova LK, Naydov IA, Novichkova NS, Ivanov BN**. **2022**. Effect of CO2 Content in Air on the Activity of Carbonic Anhydrases in Cytoplasm, Chloroplasts, and Mitochondria and the Expression Level of Carbonic Anhydrase Genes of the α- and β-Families in Arabidopsis thaliana Leaves. *Plants* **11**: 2113.

**Sage RF, Gilman IS, Smith JCA, Silvera K, Edwards EJ**. **2023**. Atmospheric CO2 decline and the timing of CAM plant evolution. *Annals of Botany* **132**: 753–770.

**Sarkar D, Kundu S**. **2025**. Water-saving guard cell-mesophyll cell model captures temporally differential enzymatic and transporter activities during C3-crassulacean acid metabolism transition. *Plant physiology* **197**: kiaf048.

**Shaw R, Cheung CYM**. **2018**. A dynamic multi-tissue flux balance model captures carbon and nitrogen metabolism and optimal resource partitioning during arabidopsis growth. *Frontiers in Plant Science* **9**: 884.

**Shen S, Li N, Wang Y, Zhou R, Sun P, Lin H, Chen W, Yu T, Liu Z, Wang Z, *et al.* 2022**. High-quality ice plant reference genome analysis provides insights into genome evolution and allows exploration of genes involved in the transition from C3 to CAM pathways. *Plant Biotechnology Journal* **20**: 2107–2122.

**Silvera K, Neubig KM, Whitten WM, Williams NH, Winter K, Cushman JC**. **2010**. Evolution along the crassulacean acid metabolism continuum. *Functional Plant Biology* **37**: 995–1010.

**Tan B, Chen S**. **2023**. Defining Mechanisms of C3 to CAM Photosynthesis Transition toward Enhancing Crop Stress Resilience. *International Journal of Molecular Sciences* **24**: 13072.

**Tay IYY, Odang KB, Cheung CYM**. **2021**. Metabolic Modeling of the C3-CAM Continuum Revealed the Establishment of a Starch/Sugar-Malate Cycle in CAM Evolution. *Frontiers in Plant Science* **11**: 573197.

**Töpfer N, Braam T, Shameer S, Ratcliffe RG, Sweetlove LJ**. **2020**. Alternative crassulacean acid metabolism modes provide environment-specific water-saving benefits in a leaf metabolic model. *Plant Cell* **32**: 3689–3705.

**Wakamatsu A, Mori IC, Matsuura T, Taniwaki Y, Ishii R, Yoshida R**. **2021**. Possible roles for phytohormones in controlling the stomatal behavior of Mesembryanthemum crystallinum during the salt-induced transition from C3 to crassulacean acid metabolism. *Journal of Plant Physiology* **262**: 153448.

**Wang X, Kraatz B, Meng J, Carrapa B, Decelles P, Clementz M, Abdulov S, Chen FH**. **2016**. Central Asian aridification during the late Eocene to early Miocene inferred from preliminary study of shallow marine-eolian sedimentary rocks from northeastern Tajik Basin. *Science China Earth Sciences* **59**: 1242–1257.

**Wang H, Wu F, Yang L, Fang X**. **2023**. Miocene lake evolution in the western Qaidam Basin, northern Tibetan Plateau: Evidence from aquatic-plant pollen. *Journal of Asian Earth Sciences* **250**: 105634.

**Winter K, Holtum JAM**. **2024**. Shifting photosynthesis between the fast and slow lane: Facultative CAM and water-deficit stress. *Journal of Plant Physiology* **294**: 154185.

**Winter K, Smith JAC**. **2022**. CAM photosynthesis: the acid test. *New Phytologist* **233**: 599–609.

## Supporting information

**Supporting Information File.** This file contains **Supporting Information Figs. S1-S7, Supporting Information Tables S1, S2** and **Supporting Information Notes S1-S4.**

**Supporting Information Dataset S1.** The model file in excel format.

**Supporting Information Dataset S2.** The model file in sbml format.

**Supporting Information Dataset S3.** Flux solutions i) for each step of $C_3$-to-CAM transition due to changes in atmospheric conditions between early-Eocene to early-Miocene and ii) for each point of the transition due to reduced transpirational water loss studied at each step of the atmospheric changes.

**Supporting Information Dataset S4.** Flux solutions obtained from simulating the model with different T (22-35°C) and RH (30-70%) at a fixed $[CO_2]_a$ of 800 ppm.

**Supporting Information Dataset S5.** Flux solutions obtained from simulating the model under different reduced $[CO_2]_a$ values at fixed T (35°C) and RH (70%).

**Supporting Information Dataset S6.** Correlation values of each reaction i) with change in atmospheric conditions (reduced $[CO_2]_a$, T and RH) between early-Eocene to early-Miocene and ii) with reduced transpirational water loss at each step of the atmospheric changes between that geological time interval.

**Supporting Information Dataset S7.** Flux solutions obtained from simulating the model by reducing RH from 80% to 40% with different combinations of T (26-35°C) and $[CO_2]_a$ (800, 419 and 250 ppm), either keeping the water loss free or keeping the water loss fixed at a value obtained with 80% RH for the corresponding T and $[CO_2]_a$ values.

**Supporting Information Dataset S8.** Flux solutions obtained from simulating the model i) at 80% RH without compromising the phloem sap production and ii) with RH reduced from 70% to 40% along with a reduced phloem sap at different T (26-35°C) under a fixed $[CO_2]_a$ of 250 ppm, either keeping the water loss free or keeping the water loss fixed at a value obtained with 80% RH for the corresponding T.

**Supporting Information Dataset S9.** The model file including additional osmolytes (nitrate, glucose, fructose and maltose) and transfer metabolites (glucose and malate) in excel format.

**Supporting Information Dataset S10.** Flux solutions by simulating the model with additional osmolytes and transfer metabolites i) for each step of $C_3$-to-CAM transition due to changes in atmospheric conditions between early-Eocene to early-Miocene and ii) for each point of the transition due to reduced transpirational water loss studied at each step of the atmospheric changes.

**Supporting Information Dataset S11.** Python scripts for all the simulations.

**Supporting Information Fig. S1.** Schematic representation of the model and constraints and flowcharts for simulating the model.

**Supporting Information Fig. S2.** Change in stomatal aperture size in different phases of day and night.

**Supporting Information Fig. S3**. Change in the $CO_2$ uptake at day and night.

**Supporting Information Fig. S4.** Variations in flux values of different carboxylating and decarboxylating enzymes.

**Supporting Information Fig. S5.** Variation in starch-malate cycle.

**Supporting Information Fig. S6.** The change in water-use efficiency (WUE) at different $[CO_2]_a$ and transpirational water loss.

**Supporting Information Fig. S7.** Variation in the diffusion coefficient of $CO_2$ ($D_{CO_2}$) with temperature (T).

**Supporting Information Table S1.** Comparison of flux values through some specific reactions of CAM under different $[CO_2]_a$ values.

**Supporting Information Table S2.** Different constraints used for GC and MC throughout the $C_3$-CAM transition.

**Supporting Information Note S1.** Increased flux of TCA cycle enzymes and $O_2$ uptake with the emergence of CAM.

**Supporting Information Note S2.** Capturing possible changes in temporal differential activities of metabolic enzymes and transporters during early-Eocene to early-Miocene time period.

**Supporting Information Note S3.** Simulating $C_3$ and CAM under predicted atmospheric changes in future.

**Supporting Information Note S4.** Simulating the model considering all potential osmolytes and transfer metabolites.

**Acknowledgements**

DS thanks Department of Biotechnology, Government of India for her fellowship.

**Competing interests**

The authors declare that there is no competing interest.

**Author contributions**

DS and SK designed the study, DS performed the simulations, both interpreted the results and co-wrote the paper.

**Figures with legends**

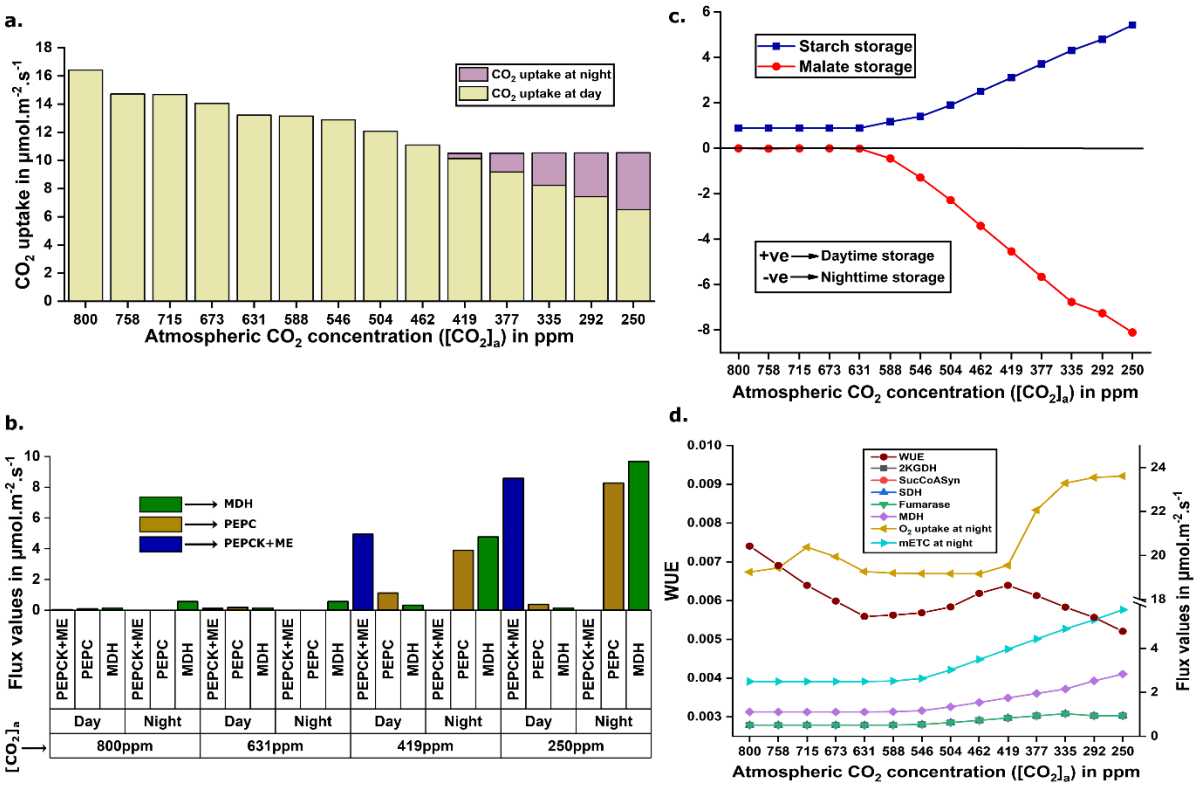


**Fig. 1.** Reduced $[CO_2]_a$ can induce CAM. **a.** Variation in the total $CO_2$ uptake throughout the diel cycle and the amount of $CO_2$ uptake at day and night with the decrease in $[CO_2]_a$. Total $CO_2$ uptake declined due to refixation of respiratory $CO_2$ (discussed in detail in main text). **b.** Changes in the activities of four $C_4$-like enzymes related to carboxylation (PEPC and MDH) and decarboxylation (PEPCK and ME) of malate at night and day respectively with the decline in $[CO_2]_a$ that show the metabolic shift towards CAM. **c.** The graph demonstrates that the daytime starch storage and the nighttime malate storage are increased throughout the C3-to-CAM transition (high to low $[CO_2]_a$). **d.** Flux through mETC and 5 enzymes of TCA cycle in MC and changes in WUE, total nocturnal $O_2$ uptake at night are shown. Flux values of 2KGDH, SucCoASyn, SDH and fumarase overlap. Only $[CO_2]_a$ values are shown in all the graphs. Corresponding T and RH values are listed in **Supporting Information Fig. S1c**.

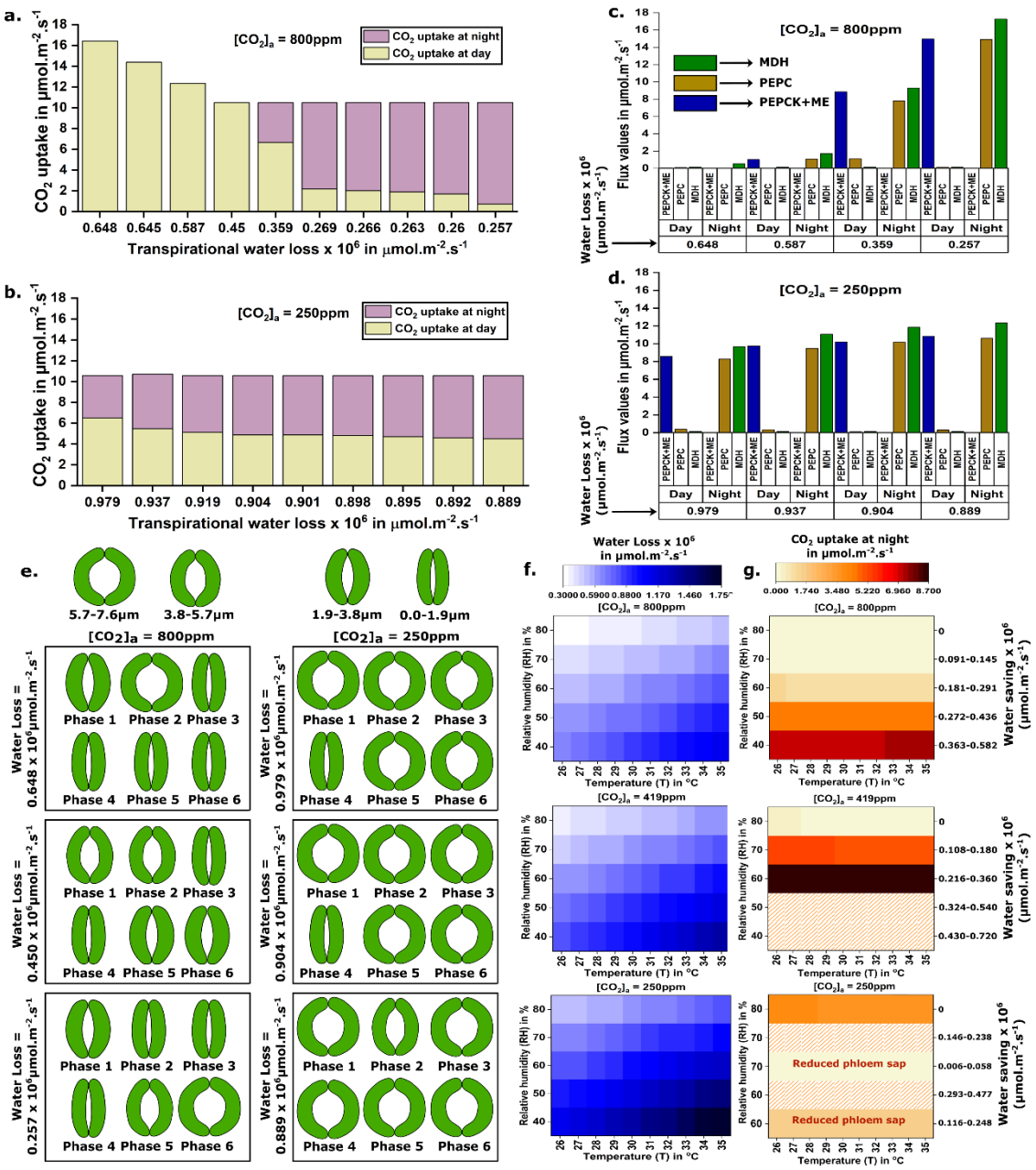


**Fig. 2. a-b** show the variation in $CO_2$ uptake at day and night with reduction in transpirational water loss at different $[CO_2]_a$. **c-d** show the changes in the activities of the carboxylating (PEPC and MDH) and decarboxylating (PEPCK and ME) enzymes with reduced transpirational water loss at different $[CO_2]_a$. **e.** Variations in stomatal aperture sizes at day and night with decline in $[CO_2]_a$ (row-wise) and transpirational water loss (column-wise) are shown. Reduced $[CO_2]_a$ forces the nighttime stomatal opening along with day, however, at a fixed $[CO_2]_a$, stomatal opening shifts from day to night with the decrease in transpirational water loss. **f.** Variation in transpirational water loss in different combinations of $[CO_2]_a$, T and RH. Water loss increases with decrease in $[CO_2]_a$, RH and increase in T. **g** shows that for a fixed T and $[CO_2]_a$, maintaining constant transpirational water loss leads to increase in nocturnal $CO_2$ uptake with decreasing RH, indicating the emergence of CAM under increasing aridity. Moreover,

at lower $CO_2$, increasing aridity (reducing RH) forces the plant to reduce its phloem sap production, showing a trade-off between water saving and phloem sap production. Only $[CO_2]_a$ values are shown in the graphs (a-e). Corresponding T and RH values are listed in **Supporting Information Fig. S1c**.